Passivity Analysis of Quadrotor Aircraft for Physical Interactions

Conference Paper · October 2021

DOI: 10.1109/AIRPHARO52252.2021.9571055

4 authors, including:

Jonathon E. Slightam
Sandia National Laboratories
27 PUBLICATIONS **172** CITATIONS

Passivity Analysis of Quadrotor Aircraft for Physical Interactions

Jonathon E. Slightam, Daniel R. McArthur, Steven J. Spencer, Stephen P. Buerger

***Abstract*— The broad dissemination of unmanned aerial vehicles (UAVs), specifically quadrotor aircraft, has accelerated their successful use in a wide range of industrial, military, and agricultural applications. Research in the growing field of aerial manipulation (AM) faces many challenges but may enable the next generation of UAV applications. The physical contact required to perform AM tasks results in dynamic coupling with the environment, which may lead to instability with devastating consequences for a UAV in flight. Considering these concerns, this work seeks to determine whether off-the-shelf flight controllers for quadrotor UAVs are suitable for AM applications by investigating the passivity and coupled-stability of quadrotors using generic cascaded position-attitude (CPA) and PX4 flight controllers. Using a planar 3-degree of freedom (DOF) linearized state-space model and two high fidelity 6-DOF models with the CPA and PX4 closed-loop flight controllers, passivity is analyzed during free flight, and stability is analyzed when the UAV is coupled to environments with varying degrees of stiffness. This analysis indicates that quadrotors using the CPA and PX4 flight controllers are non-passive (except for the PX4 controller in the vertical direction with certain vehicle parameters) and may become unstable when the UAV is coupled with environments of certain stiffnesses. Similarities between the results from the linearized 3-DOF model and nonlinear 6-DOF models in the passivity analysis suggest that using an analytical, linear approach is sufficient and potentially useful for vehicle geometry and controller design to improve stability for AM applications.**

I. Introduction

Aerial manipulation (AM) is an emerging sub-discipline of mobile robotic manipulation. Manipulation with UAVs is advantageous in that they can traverse quickly over extreme terrain, reach locations not plausible without specialized equipment, and offer payload deliveries whereas unmanned ground vehicles (UGVs) cannot. This allows for the possibility of numerous applications, some new, as depicted in Fig. 1.

This manuscript seeks to determine whether off-the-shelf flight controllers for quadrotor UAVs are suitable for AM applications by investigating the passivity of quadrotors using generic cascaded position-attitude (CPA) and PX4 flight controllers. In this investigation, we consider linearized planar and nonlinear 6-degree of freedom (DOF) quadrotor models both in free flight and when coupled to the environment, and report our findings.

This work was supported by Laboratory Directed Research and Development program at Sandia National Laboratories. Sandia National Laboratories is a multi-mission laboratory managed and operated by National Technology & Engineering Solutions of Sandia, LLC., a wholly owned subsidiary of Honeywell International, Inc., for the U.S. Department of Energy's National Nuclear Security Administration under contract DE-NA000352. This paper describes objective technical results and analysis. Any subjective views or opinions that might be expressed in the paper do not necessarily represent the views of the U.S. Department of Energy or the United States Government. All authors are with the department of Unmanned Systems and Autonomy Research and Development at Sandia National Laboratories, Albuquerque, NM, 87123 USA. [emails: jslight@sandia.gov, dmcarth@sandia.gov, sjspenc@sandia.gov, sbuerge@sandia.gov]

Fig. 1. Plausible applications with AM.

II. Background

UAV manipulation research and development is generally divided into two categories: simple load carrying (sometimes called "flying hand" approaches), and rich, multi-DOF manipulation. To date, industry investments have focused primarily on load carrying, which is a much simpler problem. This work has been extended to study the dynamics of suspended loads [1]. Counter-UAV work at Sandia National Laboratories has included capturing and carrying a "red force" UAV in a net suspended from four "blue force" UAVs [2]; even in this relatively simple case, stability and drift problems emerged from contact dynamics. Current state-of-the-art AM efforts with multi-DOF arms have demonstrated some level of success within controlled laboratory environments and experimental setups [3]–[6]. Experiments include pick and place, assembly/disassembly, and constrained manipulation, e.g., turning a valve or knob. Quantitative performance indices such as position errors for the aerial platforms and manipulators indicate that task complexity beyond pick and place operations cannot be achieved autonomously in most realistic field operation scenarios. For example, Park et al. reported that submillimeter peg in a hole assembly was only possible with human-in-the-loop teleoperation [5]. Other researchers reported position errors typically greater than 1 cm, which would make most dexterous manipulation and assembly/disassembly tasks nearly impossible outside of controlled laboratory experiments.

Limited development of airborne impedance controllers have been reported in simulation [7], and more recently in hardware with both underactuated [8] and fully-actuated vehicles [9]. However, these experiments do not consider

strongly coupled environment dynamics or model the dynamic imperfections (e.g. structural modes) that often cause stability and performance problems. At least one group has examined coupling solidly to rigid environments, in this case a valve [6]. A switched control approach was used, and the UAV moved into a perch mode when in contact, as opposed to continuing flight.

Plausible stability issues with AM and their high consequences for critical applications motivate a fundamental investigation of quadrotor UAVs' passivity both analytically and theoretically with popular flight controllers. Passivity is a property of physical systems that can be broadly defined as how a system dissipates energy such that it is stable, and is primarily used to describe interacting systems with Port-Hamiltonian theory, e.g. a manipulator interacting with the environment.

Historically, roboticists have analyzed the passivity of manipulators, and have devised control methods to make them passive at their ports of interaction (e.g. at a gripper). In most prior cases, the base of the manipulator is assumed to be rigid. However, in the case of a controlled quadrotor in flight, the base dynamics reflect the intrinsic dynamics of the body as well as the controller that is required to stabilize flight. In light of this, understanding the impedance and passivity characteristics of a UAV may provide insight into the type of AM interactions that are feasible with that vehicle, and aid in the development of complementary manipulators and controllers for the vehicle that enable robust, stable AM interactions.

In this manuscript, we present an analytical linear 3-DOF model and two high fidelity 6-DOF numerical models of quadrotor UAVs that employ CPA and PX4 flight controllers in Section III. The theory used for analyzing the passivity of the vehicles during flight and when coupled to the environment is presented in Section IV. Passivity analysis results are reported in Section V, followed by discussions and conclusions in Sections VI and VII, respectively.

III. Dynamics and Control of Quadrotor Aircraft

This section presents a linearized analytical 3-DOF model and two high fidelity 6-DOF numerical models using both MATLAB/Simulink and Gazebo. The CPA and PX4 flight controllers used for analysis are also introduced here.

A. 3-DOF Linear State-Space Model

We derive the equations of motion (EOM) of a quadrotor UAV in linear state-space form to enable passivity analysis for different flight controllers and gain insights in ways numerical methods cannot. The second order EOMs are derived from the planar model of the UAV illustrated in Fig. 2 using Newton's second law. We assume a rigid body dynamic model for the aircraft.

Using Newton's second law we describe the motion of the vehicle due to the thrust of the left and right propellers and external force in the global x-direction as follows

$$m\ddot{x} = -(F_1 + F_2)\sin\theta + F_x \tag{1}$$

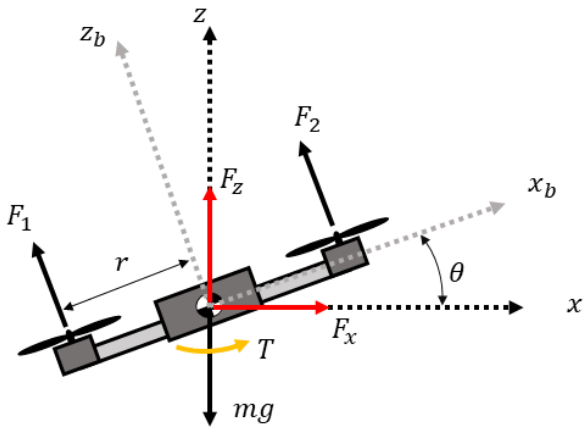

Fig. 2. Planar (3-DOF) rigid body dynamic model of a quadrotor UAV.

where m is the total mass of the vehicle, F_1 is the thrust provided by the left prop-rotor assembly, F_2 is the thrust provided by the right prop-rotor assembly, θ is the pitch of the UAV, and F_x is the external force exerted on the UAV through the center of mass in the global frame's x-direction.

Similarly, we describe the motion of the UAV in the vertical (z) direction including gravity with

$$m\ddot{z} = (F_1 + F_2)\cos\theta - mg + F_z \tag{2}$$

where g is the acceleration due to gravity and F_z is the external force exerted on the UAV through the center of mass in the global frame's z-direction.

The angular motion about the UAV center of mass is described by the torque generated from the thrust difference between propellers 2, and 1, and the externally applied torque to the vehicle about the center of mass, giving

$$I\ddot{\theta} = r(F_2 - F_1) + T \tag{3}$$

where I is the inertia of the UAV, r is the radius from the center of mass to the propeller centers, and T is the external torque exerted on the UAV about the center of mass.

To write (1)-(3) in state-space form we let $x = x_1$, $\dot{x} = x_2$, $z = x_3$, $\dot{z} = x_4$, $\theta = x_5$, and $\dot{\theta} = x_6$. These assertions allow us to write the state equations for the x-direction as

$$\dot{x}_1 = x_2, \quad \dot{x}_2 = \frac{1}{m}\Big(-(F_1 + F_2)\sin x_5 + F_x\Big), \tag{4}$$

the EOM in the z-direction as

$$\dot{x}_3 = x_4, \quad \dot{x}_4 = \frac{1}{m}\Big((F_1 + F_2)\cos x_5 + F_z\Big) - g, \tag{5}$$

and the EOM in the angular component about the center of mass as

$$\dot{x}_5 = x_6, \quad \dot{x}_6 = \frac{1}{I}\Big(r(F_2 - F_1) + T\Big). \tag{6}$$

Linearization of (4)-(6) further enables the state-space form to be put into a linear time-invariant (LTI) form:

$$\begin{aligned} \dot{x} &= \mathbf{A}x + \mathbf{B}u \\ y &= \mathbf{C}x + \mathbf{D}u \end{aligned} \tag{7}$$

For the system inputs of (4)-(6), we define $u_1 = F_1 + F_2$, $u_2 = r(F_2 - F_1)$, $u_3 = F_x$, $u_4 = F_z - mg$, and $u_5 = T$. For linearization of (4), we introduce a nominal thrust gain, $K_{u1} \approx u_1$, for equilibrium flight and assume small angle approximation for the sine term, resulting in

$$\dot{x}_2 = \frac{1}{m}\Big(-K_{u_1}x_5 + u_3\Big). \tag{8}$$

For linearization in the z-direction (vertical), we use the small angle approximation for cosine resulting in

$$\dot{x}_4 = \frac{1}{m}\Big(u_1 + u_4\Big). \tag{9}$$

With the prior definitions, the angular motion of the UAV can be rewritten as

$$\dot{x}_6 = \frac{1}{I}\Big(u_2 + u_5\Big). \tag{10}$$

Consolidating appropriate terms into the matrices **A**, **B**, and **C** gives

$$\mathbf{A} = \begin{bmatrix} 0 & 1 & 0 & 0 & 0 & 0 \\ 0 & 0 & 0 & 0 & -K_{u_1}/m & 0 \\ 0 & 0 & 0 & 1 & 0 & 0 \\ 0 & 0 & 0 & 0 & 0 & 0 \\ 0 & 0 & 0 & 0 & 0 & 1 \\ 0 & 0 & 0 & 0 & 0 & 0 \end{bmatrix}, \tag{11}$$

$$\mathbf{B} = \begin{bmatrix} 0 & 0 & 0 & 0 & 0 \\ 0 & 0 & 1/m & 0 & 0 \\ 0 & 0 & 0 & 0 & 0 \\ 1/m & 0 & 0 & 1/m & 0 \\ 0 & 0 & 0 & 0 & 0 \\ 0 & 1/I & 0 & 0 & 1/I \end{bmatrix}, \tag{12}$$

and

$$\mathbf{C} = \begin{bmatrix} 1 & 0 & 0 & 0 & 0 & 0 \\ 0 & 1 & 0 & 0 & 0 & 0 \\ 0 & 0 & 1 & 0 & 0 & 0 \\ 0 & 0 & 0 & 1 & 0 & 0 \\ 0 & 0 & 0 & 0 & 1 & 0 \\ 0 & 0 & 0 & 0 & 0 & 1 \end{bmatrix}, \tag{13}$$

and $\mathbf{D} = \mathbf{0}$.

The dynamics of the simplified 3-DOF UAV modeled in LTI form can be used with MATLAB's Control System Toolbox to analyze the behavior of the dynamic system with flight controllers.

B. 6-DOF High Fidelity Models

In addition to analyzing reduced-order models, full 6-DOF models of flight vehicle dynamics and controllers were also considered. This enabled validation of the reduced-order models, potential exposure of more complex dynamic couplings and interactions than could be shown with the planar models, and direct comparison with prior literature that leveraged the same models.

UAV flights were simulated in both Gazebo and Simulink to generate data for analysis. The Simulink model is based on the Parrot Mambo quadcopter airframe, uses a complementary filter to estimate attitude, Kalman filters to estimate position and velocity, and implements the CPA flight controller, which is described in more detail below. The Gazebo model is based on the 3DR Iris quadcopter airframe, uses an extended Kalman filter (EKF) to estimate vehicle attitude, position and velocity, and implements the PX4 flight controller (also described in more detail below) in conjunction with robot models and Gazebo plugins (e.g. for computing thrust from rotor velocities) provided by the developers of the PX4 flight stack.

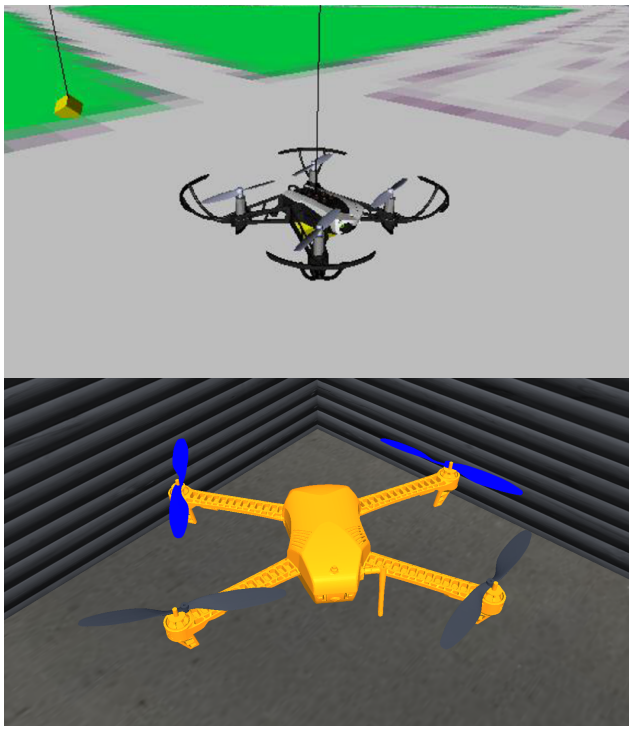

Fig. 3. 6-DOF high fidelity model of Mambo quadrotor UAV in Simulink (top) and 3DR Iris quadrotor UAV in Gazebo (bottom).

The numeric complexity inherent in these higher-order simulations requires different methods to enable passivity analysis. To determine key transfer functions, such as impedance or admittance functions that describe behavior of the controlled nonlinear flight system at points of physical interaction with the environment, system identification methods were used. Specifically, external force profiles were imposed at the point of interaction with the controlled flight vehicle (center of gravity (CG)), and the resulting motions were "measured" in simulation. The relationships between these input and output variables were then quantified. Interactions were considered only at the CG since the UAV is treated as a rigid body, and thus any interactions that are not through the CG can be transformed into an equivalent wrench applied at the CG.

For example, input signals consisting of summations of sinusoids (hereafter referred to as *multisine* inputs) were applied, and Fast Fourier Transforms (FFTs) were computed for both the input and output signals. By comparing the

frequency content of the input and output, the approximate (linearized) dynamic behavior was estimated. Using this method, the full 6x6 impedance (or admittance) matrix may be derived at a point of interaction.

C. CPA & PX4 Flight Controllers

The open-source PX4 autopilot flight stack software employs a cascaded position-attitude rate controller (see Fig. 4, bottom, for a block diagram of the PX4 controller reduced to 3-DOF). The position controller includes proportional position control paired with PI+D velocity control. Similarly, the attitude controller includes proportional control over the angular position, and PI+D control for the angular rates.

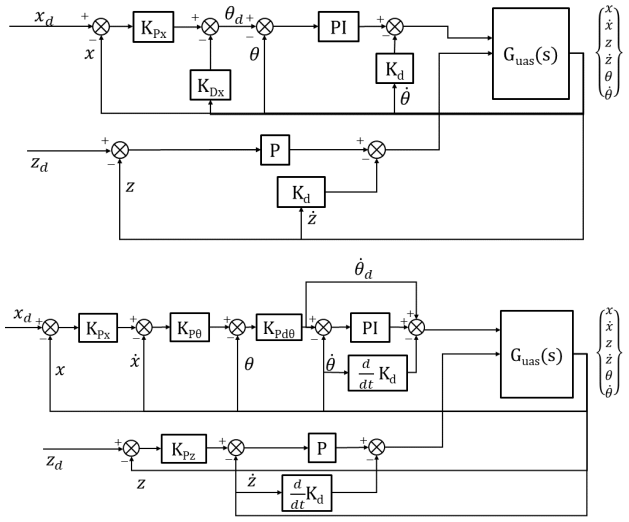

Fig. 4. Block diagram of the cascaded position-attitude flight controller (top) and the PX4 cascaded position-attitude rate controller (bottom) reduced to 3-DOF [10].

The CPA controller implements a simpler PD- and PI-type control system for altitude and attitude control, respectively, as shown in the top of Fig. 4.

In the following sections, the 3-DOF Parrot Mambo model paired with the CPA controller will be referred to as the $3D_{CPA}$ model, and the 3-DOF Parrot Mambo model with the PX4 controller will be referred to as the $3D_{PX4}$ model. Similarly, the 6-DOF Parrot Mambo model with the CPA controller will be referred to as the $6D_{CPA}$ model, and the 6-DOF 3DR Iris model with the PX4 controller will be referred to as the $6D_{PX4}$ model.

IV. Passivity Analysis

Passivity analysis views system stability through the lens of port interaction behavior, i.e., how energy is exchanged through ports of interaction or impedance and admittance [11], [12]. As it pertains to manipulation systems, the key property of systems with "passive" ports of physical interaction is that, when coupled to other passive systems through a passive port, the coupled system is stable. All combinations of inertial, compliant, and dissipative elements are passive; therefore, a manipulator that exhibits passivity is guaranteed to be stable when interacting with an extraordinarily large set of environments - indeed any physical system that cannot, itself, inject net energy into the interface. Applying this analysis to UAVs allows us to determine whether there are fundamental challenges introduced by current UAV flight controllers in the context of AM.

A system is passive if the real components of the complex impedance or admittance are strictly positive,

$$Re(Y(j\omega)) \geq 0 \quad and \quad Re(Z(j\omega)) \geq 0 \tag{14}$$

Equation (14) can be used for characterizing the passivity of a UAV during normal flight.

A. Passivity Definition for Coupled Interactions

Passivity analysis can help determine if there are stability issues when the UAV becomes coupled with the environment. At the port of interaction, we'll represent the UAV with its admittance Y, and the environment with its impedance Z. We apply the concept of "worst-case" environments [11], which are always either pure masses or springs, because they don't have any dissipative properties. Specifically, we consider interactions with springs that are expected to produce instability. Fig. 5 shows the stability analysis workflow where Fig. 5 (a) is a two-dimensional UAV grasping a peg protruding from the ground, which can be modeled as shown in Fig. 5 (b), and this port interaction behavior can be represented by the block diagram shown in Fig. 5 (c).

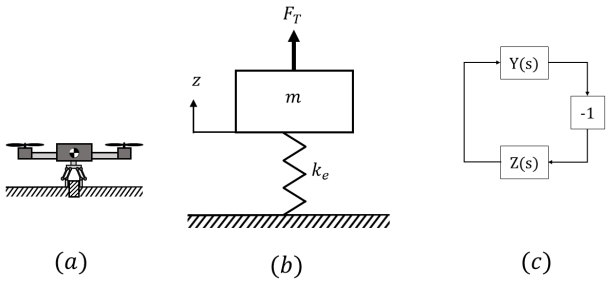

Fig. 5. Passivity analysis workflow for UAV coupled to spring environment. (a) UAV grasping a peg; (b) simplified representation of a UAV coupled to the environment; (c) block diagram of UAV/environment port interaction.

The closed-loop behavior shown in Fig. 5 (c) can be represented by

$$G(j\omega)_{CL} = \frac{Y(j\omega)_{UAV} Z(j\omega)_{env}}{1 + Y(j\omega)_{UAV} Z(j\omega)_{env}} \tag{15}$$

where (15) represents the closed-loop coupled system. As in classical analysis of single-input, single-output control systems, analysis of the open-loop transfer function, (16), provides key insights about the behavior of the closed-loop coupled system.

$$G(j\omega)_{OL} = Y(j\omega)_{UAV} Z(j\omega)_{env} \tag{16}$$

Specifically, instability is indicated by the Nyquist stability criterion if the point [-1, 0] is encircled in the real-imaginary plane as ω is varied from $-\infty$ to ∞ in $G(j\omega)_{OL}$.

V. Simulation Results

Several simulations of the $3D_{CPA}$, $3D_{PX4}$, $6D_{CPA}$ and $6D_{PX4}$ models (defined in Section III-C above) were conducted to assess the passivity of the Parrot Mambo and 3DR Iris quadrotor airframes. The $3D_{CPA}$, $3D_{PX4}$, and $6D_{CPA}$ models were simulated in the MATLAB/Simulink environment (for the Parrot Mambo airframe), and the $6D_{PX4}$ model was simulated in the Gazebo environment (for the 3DR Iris airframe).

Using the simulation data, the impedance of each UAV was computed for all 36 combinations of force/torque inputs and linear/angular velocity outputs. Each impedance is denoted by $Z(s)_{F\to V} = F(s)/V(s)$ where $F(s)$ is the input force or torque, and $V(s)$ is the linear or angular velocity output.

A. Passivity of a Hovering UAV

1) Linearized 3-DOF Models: The $3D_{CPA}$ and $3D_{PX4}$ models were implemented in MATLAB using the Control System Toolbox with the matrix of the closed-loop transfer functions of impedance and admittance found using the *connect* function. Linear, second-order motor dynamics were added using this function as well. These simulations used the vehicle parameters of the Parrot Mambo UAV (e.g. mass, inertia, etc.) obtained from the Simulink model.

Nyquist plots of the impedance and admittance for the $3D_{CPA}$ model are shown in Fig. 6 (vertical motion, $Z_{F_z\to V_z}$), Fig. 7 (horizontal (x) motion, $Z_{F_x\to V_x}$), and Fig. 8 (pitch motion, $Z_{T\to\dot{\theta}}$). A Nyquist plot of the impedance and admittance for the $3D_{PX4}$ model is shown in Fig. 9 (vertical motion, $Z_{F_z\to V_z}$).

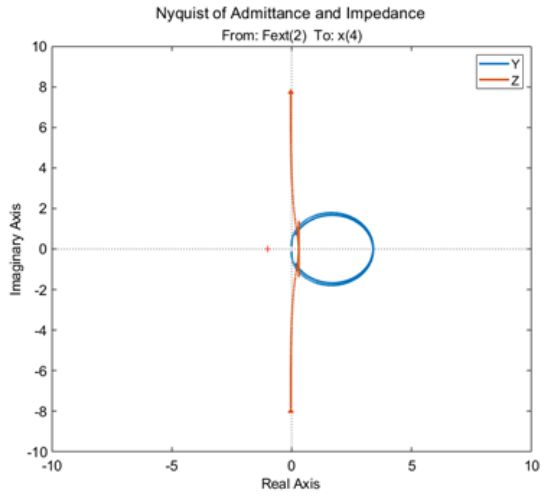

Fig. 6. Vertical component of impedance and admittance for the $3D_{CPA}$ model. A plus sign denotes the (-1,0) coordinate but is not used in this passivity analysis.

In each scenario for the $3D_{CPA}$ model, the admittance and impedance cross the imaginary axis onto the left-half plane (LHP), which indicates that the system during flight is non-passive.

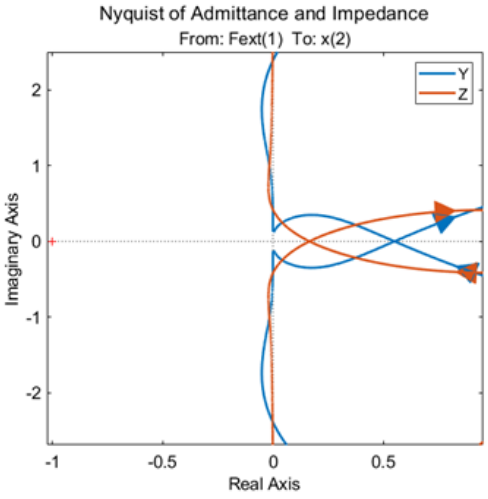

Fig. 7. Horizontal component of impedance and admittance for the $3D_{CPA}$ model.

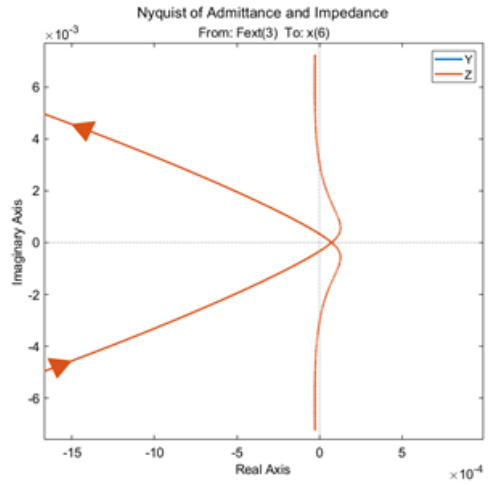

Fig. 8. Angular component of impedance and admittance for the $3D_{CPA}$ model. Admittance is not shown due to scaling.

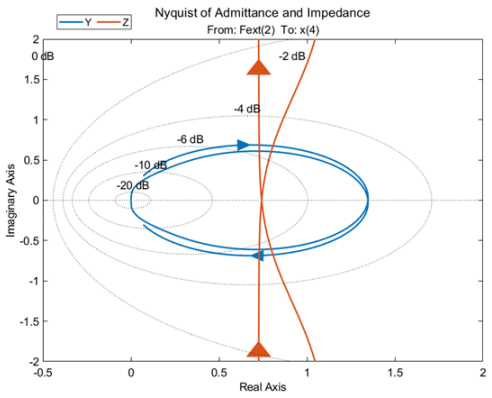

Fig. 9. Vertical component of impedance and admittance for the $3D_{PX4}$ model ($Z_{F_z\to V_z}$).

2) Full 6-DOF Models: The 6-dimensional impedance behavior of the Parrot Mambo ($6D_{CPA}$) and 3DR Iris

(6D$_{PX4}$) UAVs were estimated using the Matlab/Simulink and Gazebo environments, respectively, as follows. Multisine force and torque inputs (described in Sec. III-B) were applied at each vehicle's CG for all 6 DOF (one axis at a time), while the vehicle hovered in place. The resulting linear and angular velocities of the UAV in response to the multisine input were recorded for each time step of the simulation. The force and torque input and the velocity outputs for each simulation were converted to the discrete frequency domain using an FFT, and the impedance of the UAV was computed for all 36 combinations of force and torque inputs and linear and angular velocity outputs as noted above.

A qualitative representation of the 6x6 impedance behavior of the 6D$_{CPA}$ and 6D$_{PX4}$ models was developed by observing the Nyquist plot for each of the 36 impedances described above (see Fig. 10). The only components with discernible content lie on the main diagonal or super-anti-diagonal. The four elements off of the main diagonal indicate that those components have cross-coupling between those axes. Intuitively, this pattern makes sense. Lateral forces and velocities interact with pitch and roll angular velocity and torque respectively, but all other axes are decoupled.

$$\begin{bmatrix} F_x \to V_x & F_x \to V_y & F_x \to V_z & F_x \to \omega_x & F_x \to \omega_y & F_x \to \omega_z \\ F_y \to V_x & F_y \to V_y & F_y \to V_z & F_y \to \omega_x & F_y \to \omega_y & F_y \to \omega_z \\ F_z \to V_x & F_z \to V_y & F_z \to V_z & F_z \to \omega_x & F_z \to \omega_y & F_z \to \omega_z \\ \tau_x \to V_x & \tau_x \to V_y & \tau_x \to V_z & \tau_x \to \omega_x & \tau_x \to \omega_y & \tau_x \to \omega_z \\ \tau_y \to V_x & \tau_y \to V_y & \tau_y \to V_z & \tau_y \to \omega_x & \tau_y \to \omega_y & \tau_y \to \omega_z \\ \tau_z \to V_x & \tau_z \to V_y & \tau_z \to V_z & \tau_z \to \omega_x & \tau_z \to \omega_y & \tau_z \to \omega_z \end{bmatrix}$$

Fig. 10. Visualization of axis coupling between force/torque inputs and velocity outputs for 6D$_{CPA}$ and 6D$_{PX4}$ models (Parrot Mambo and 3DR Iris UAVs). Green entries represent terms with discernible content in the Nyquist plot of the impedance.

For conciseness, key impedance plots for the 6D$_{CPA}$ model are presented here, most of which correspond to the plots shown above for the 3D$_{CPA}$ model, for comparison.

Figures 11, 12, and 13, show the Nyquist plots of the 6D$_{CPA}$ model's impedance for vertical, horizontal (forward), and pitch motions: $Z_{F_z \to V_z}$, $Z_{F_x \to V_x}$, and $Z_{\tau_y \to \omega_y}$, respectively. Figure 14 shows the Nyquist plot of the 6D$_{CPA}$ model's yaw impedance.

B. Stability with Environment Coupling

The 3D$_{CPA}$, 6D$_{CPA}$, and 6D$_{PX4}$ models were simulated to analyze the stability of the UAVs when coupled to a spring environment with a range of stiffnesses in the horizontal and vertical directions. This analysis serves to demonstrate that the non-passive UAV system does, in fact result in unstable contact with some environments, e.g. "worst-case" environments as described in section IV. As a result, stability boundaries can be defined in the space of the environment dynamics. Equation (16) is used to create a Nyquist plot to determine when the interaction results in instability, i.e., encirclement of the (-1,0) point.

Fig. 15 and Fig. 16 show the Nyquist plot of the open-loop coupled system $Z_{env}Y_{UAV}$ comprised of the 3D$_{CPA}$ and 6D$_{CPA}$ model quadrotors connected to the environment

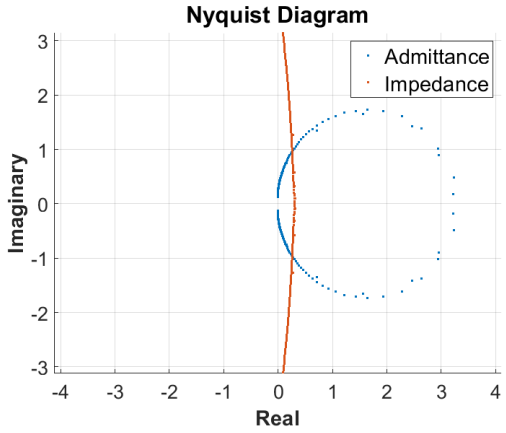

Fig. 11. Vertical direction impedance ($Z_{F_z \to V_z}$) for the 6D$_{CPA}$ model (Parrot Mambo).

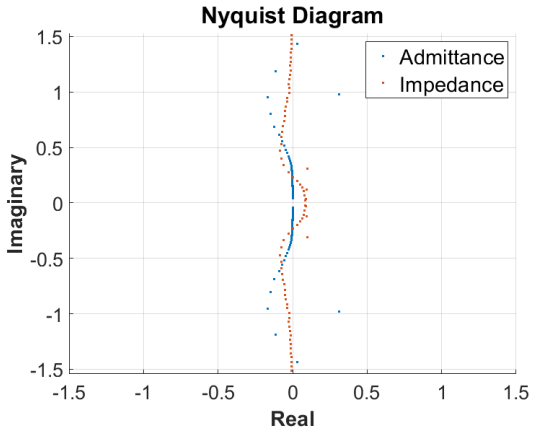

Fig. 12. Horizontal (forward) direction impedance ($Z_{F_x \to V_x}$) for the 6D$_{CPA}$ model (Parrot Mambo).

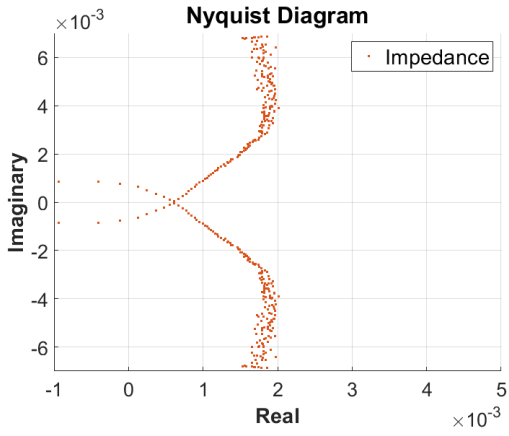

Fig. 13. Pitch impedance ($Z_{\tau_x \to \omega_x}$) for the 6D$_{CPA}$ model (Parrot Mambo).

via a spring attached at the UAV's CG oriented along the body z axis (vertical direction). Z_{env} is the impedance of the environment (spring): $k/j\omega$ and Y_{UAV} is the admittance of the UAV: Z_{UAV}^{-1}.

Additional simulations were performed with the 3D$_{CPA}$,

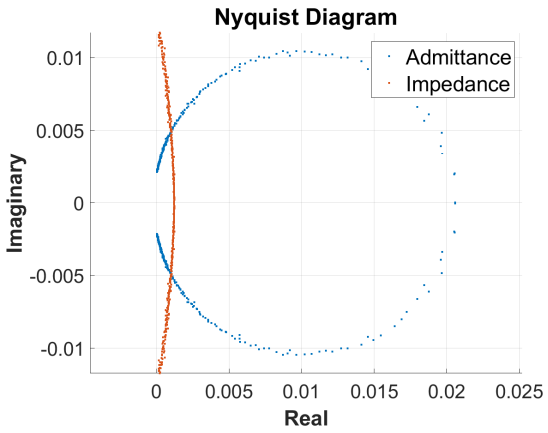

Fig. 14. Yaw impedance ($Z_{T_z \to \omega_z}$) for the 6D$_{CPA}$ model (Parrot Mambo).

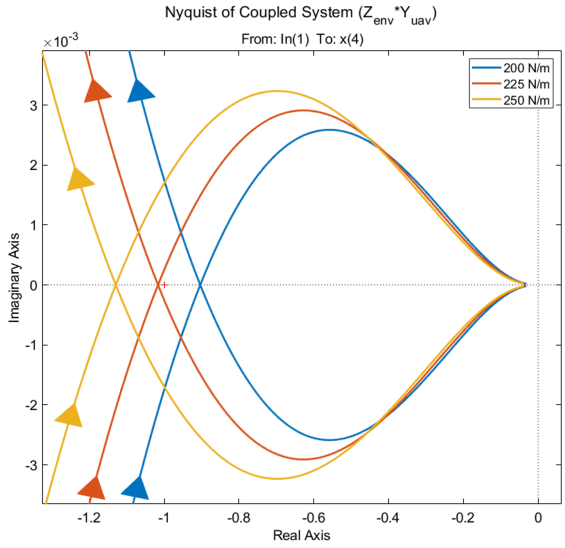

Fig. 15. Nyquist plot of the coupled impedance of the 3D$_{CPA}$ model (Parrot Mambo) connected to the environment in the vertical axis (Z-axis) with a range of spring stiffnesses. Note the encirclement of the point (-1, 0) for $k >\approx 220 N/m$, indicating instability.

6D$_{CPA}$ and 6D$_{PX4}$ models coupled via springs in the horizontal (x) and vertical (z) directions (separately). The results of those simulations were similar to what is shown in Fig. 15 and Fig. 16.

VI. Discussion

In this work, we primarily set out to determine whether off-the-shelf flight controllers for quadcopter UAVs result in passive vehicle dynamics for interactions with the environment. Because controlled quadrotors exhibit several unique behaviors, such as coupled dynamics between translation and rotational axes resulting from underactuation, we hypothesized that controlled flight bodies would be non-passive.

Through our simulated analysis of the 3D$_{CPA}$, 3D$_{PX4}$, 6D$_{CPA}$ and 6D$_{PX4}$ models, we found that off-the-shelf flight controllers do indeed create non-passive vehicle dynamics, as indicated by portions of the impedance/admittance

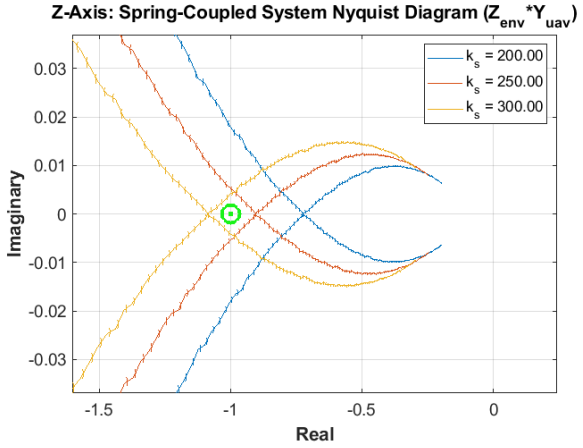

Fig. 16. Nyquist plot of the coupled impedance of the 6D$_{CPA}$ model (Parrot Mambo) connected to the environment in the vertical axis (Z-axis) with a range of spring stiffnesses. Note the encirclement of the point (-1, 0) for $k >\approx 275 N/m$, indicating instability.

plots crossing into the left-half plane of the Nyquist plots. Two notable exceptions are the 3D$_{PX4}$ model in the vertical direction (see Fig. 9) and the 6D$_{CPA}$ model in the yaw direction (see Fig. 14).

As noted previously, many of the cross-axis terms in the 6x6 impedance matrix for the 6D$_{CPA}$ and 6D$_{PX4}$ models (Fig. 10) have no discernible or consistent impedance behavior (indicated by red text). This is not surprising, and indicates primarily that there is little coupling between these axes. For instance, it is not surprising that a pure torque applied around the z-axis (the vertical axis of the vehicle) is independent of lateral motion, rotation about other vehicle axes, etc. This result indicates that the complex controlled dynamics of quadrotors can be distilled to their effective dynamics at the point of interaction. These dynamics may then be analyzed for stability and performance (in this case, representation of desired impedance). The lack of coupling suggests that each axis impedance can be considered independently.

A strong similarity was observed between the shapes of the impedance curves derived analytically for the linear 3-DOF models and the numerically-determined curves for the 6-DOF models. For example, compare Fig. 6 and 11, Fig. 8 and 13, and Fig. 15 and 16. These similarities suggest that simplified analytical models can provide insightful analysis to drive new controller and hardware designs to ensure passivity.

As suspected, the non-passivity of the different vehicles and flight controllers results in predictable transitions to instabilities when coupled to increasing spring stiffnesses as indicated in Fig. 15 and 16. In general, this suggests that interactions with stiff environments are likely to be challenging for multirotor manipulators while in flight. Thus, important tasks such as working against constraints (rigid walls, hinged doors, etc.) are likely to pose stability problems, which strongly motivates the design of alternative vehicles and flight controllers that specifically enable pas-

sivity, and/or controlled manipulators that compensate for non-passive vehicle dynamics and produce more favorable contact dynamics at the point of interaction.

The presented approached for analysis suggests that the methods can be used to tune controllers to improve the range of stable interactions with the environment, as the PX4 flight control architecture showed in vertical cases with certain vehicle parameters. For example, changes in the rate control gains, i.e., K_d in Fig. 4, may increase the range of stable stiffnesses during interaction.

Not considered is the impact of structural dynamic modes, specifically those that decouple the location of the contact with the environment from that of the actuators. With most quadcopter UAVs non-collocations between the propellers and flight control unit accurately reflects the fact that in most common multirotor aircraft, the motors and propellers are located at the ends of relatively compliant structural arms. This "non-collocation" problem is known to introduce stability challenges in other physically interacting / force-controlled systems. This known problem in manipulation suggests further analysis considering non-collocation and experimental validation.

VII. Conclusion

In this work, we simulated a 3-DOF linearized quadcopter model that used the CPA and PX4 flight controller architectures as well as high fidelity 6-DOF models that also used the CPA and PX4 flight controller architectures. Through the passivity analysis conducted, we found that these off-the-shelf flight controllers are non-passive, and may become unstable when coupled with environments of certain stiffnesses. Exceptions in non-passiveness were found for the Mambo ($6D_{CPA}$) yaw and the PX4 flight control architecture in the vertical case for some vehicle parameters. Passivity cases found suggests that controllers that utilize rate controllers may allow for passivity with appropriate tuning.

The non-passive behavior of off-the-shelf flight controllers suggest that their use for manipulation tasks that are rich with coupling to the environment will be problematic and likely encounter instabilities. The analysis conducted herein illustrates an approach to use passivity analysis for revised quadrotor vehicle designs and new flight controllers that are more suitable for AM.

References

[1] A. Faust, I. Palunko, P. Cruz, R. Fierro, and L. Tapia, "Learning swing-free trajectories for UAVs with a suspended load," *Proceedings - IEEE International Conference on Robotics and Automation*, pp. 4902–4909, 2013.

[2] A. P. Vinod, B. Homchaudhuri, C. Hintz, A. Parikh, S. P. Buerger, M. M. Oishi, G. Brunson, S. Ahmad, and R. Fierro, "Multiple Pursuer-Based Intercept via Forward Stochastic Reachability," *Proceedings of the American Control Conference*, vol. 2018-June, pp. 1559–1566, 2018.

[3] V. Lippiello, J. Cacace, A. Santamaria-Navarro, J. Andrade-Cetto, M. Á. Trujillo, Y. Rodríguez Esteves, and A. Viguria, "Hybrid Visual Servoing With Hierarchical Task Composition for Aerial Manipulation," *IEEE Robotics and Automation Letters*, vol. 1, no. 1, pp. 259–266, 2016.

[4] F. Ruggiero, V. Lippiello, and A. Ollero, "Aerial manipulation: A literature review," *IEEE Robotics and Automation Letters*, vol. 3, no. 3, pp. 1957–1964, 2018.

[5] S. Park, J. Lee, J. Ahn, M. Kim, J. Her, G. H. Yang, and D. Lee, "ODAR: Aerial Manipulation Platform Enabling Omnidirectional Wrench Generation," *IEEE/ASME Transactions on Mechatronics*, vol. 23, no. 4, pp. 1907–1918, 2018.

[6] M. Orsag, C. Korpela, S. Bogdan, and P. Oh, "Dexterous Aerial Robots — Mobile Manipulation," *IEEE Transactions on Robotics*, vol. 33, no. 6, pp. 1453–1466, 2017. [Online]. Available: http://ieeexplore.ieee.org/document/8059875/

[7] V. R. Lippiello and Fabio, "Exploiting Redundancy in Cartesian Impedance Control of UAVs Equipped with a Robotic Arm," in *Proceedings of the IEEE/RSJ International Conference on Intelligent Robots and Systems*, 2012, pp. 3768–3773.

[8] B. Yüksel, C. Secchi, H. H. Bülthoff, and A. Franchi, "Aerial physical interaction via IDA-PBC," *International Journal of Robotics Research*, vol. 38, no. 4, pp. 403–421, 2019.

[9] R. Rashad, F. Califano, and S. Stramigioli, "Port-Hamiltonian Passivity-Based Control on SE(3) of a Fully Actuated UAV for Aerial Physical Interaction Near-Hovering," *IEEE Robotics and Automation Letters*, vol. 4, no. 4, pp. 4378–4385, 2019.

[10] "PX4 Controller Diagrams," accessed: May 13, 2021. [Online]. Available: https://docs.px4.io/master/en/flight_stack/controller_diagrams.html

[11] J. E. Colgate and N. Hogan, "Robust control of dynamically interacting systems," *International Journal of Control*, vol. 48, no. 1, pp. 65–88, 1988.

[12] N. Hogan and S. Buerger, "Impedance and Interaction Control," in *Robotics and Automation Handbook*. Berlin, Heidelberg: CRC Press, oct 2005, ch. 19, pp. 1–24. [Online]. Available: http://www.crcnetbase.com/doi/abs/10.1201/9781420039733.ch19